Bull Math Biol
DOI 10.1007/s11538-017-0304-3

ORIGINAL ARTICLE

Mathematical and Computational Modeling for Tumor Virotherapy with Mediated Immunity

Asim Timalsina[1] · **Jianjun Paul Tian**[2] · **Jin Wang**[3]

Received: 7 June 2016 / Accepted: 26 May 2017

Abstract We propose a new mathematical modeling framework based on partial differential equations to study tumor virotherapy with mediated immunity. The model incorporates both innate and adaptive immune responses and represents the complex interaction among tumor cells, oncolytic viruses, and immune systems on a domain with a moving boundary. Using carefully designed computational methods, we conduct extensive numerical simulation to the model. The results allow us to examine tumor development under a wide range of settings and provide insight into several important aspects of the virotherapy, including the dependence of the efficacy on a few key parameters and the delay in the adaptive immunity. Our findings also suggest possible ways to improve the virotherapy for tumor treatment.

Keywords Tumor virotherapy · Innate and adaptive immune responses · Mathematical modeling

1 Introduction

Cancer is characterized by abnormal cell growth without control. Cancer cells typically grow and divide rapidly, with a high potential of invading and spreading to other parts of the body. The causes for cancer are complicated and could involve biological,

✉ Jin Wang
Jin-Wang02@utc.edu

1 Department of Mathematics and Statistics, Old Dominion University, Norfolk, VA 23529, USA

2 Department of Mathematical Sciences, New Mexico State University, Las Cruces, NM 88003, USA

3 Department of Mathematics, University of Tennessee at Chattanooga, Chattanooga, TN 37403, USA

Published online: 07 June 2017

environmental, and genetical factors, as well as related to the age, life style, and health conditions of individuals. Cancer has long been a leading cause of death in developed countries. The World Health Organization (WHO) estimates that in 2012, about 14 million new cases of cancer occurred, which led to about 8.2 million deaths (World Cancer Report 2014a). Meanwhile, there are tremendous financial costs in connection with cancer, estimated at 1.16 trillion US dollars per year as of 2010 (World Cancer Report 2014b).

There have been a number of options available for cancer management. Surgery, the primary method of treatment for most isolated cancers, aims to remove the entire tumor from the body. However, complete surgical excision is often difficult, with success mainly for small and localized tumors. The procedure may be impossible for tumors that either have metastasized to other sites of the body or possess metastatic potential. Chemotherapy, on the other hand, is the treatment of cancer with one or more drugs that can kill the tumor cells. Such anticancer drugs typically target cells that divide rapidly, an essential property of tumor cells, though healthy cells with a high replacement rate can be potentially harmed. The effectiveness of chemotherapy thus depends on the type and stage of the cancer, and the toxicity introduced to other tissues in the body. Radiation therapy, another common approach for treating cancers, utilizes ionizing radiation in an attempt to damage the genetic materials of tumor cells and prevent these cells from continuing growth and division. The radiation (inevitably) injures normal cells and tissues, as a side effect, and it is often used in combination with surgery and/or chemotherapy. Other tumor treatment options include, but not limited to, hormonal therapy, immunotherapy, angiogenesis inhibitors, and palliative care.

A relatively new, yet propitious, strategy in treating cancer is the virotherapy (Shah et al. 2003; Marchini et al. 2016), which makes use of genetically engineered oncolytic viruses that are specific to tumor cells. Once entering the tumor (typically through intralesional injection), the oncolytic viruses infect cancer cells and replicate inside them, while leaving normal cells and tissues unharmed. Through the lysis of the infected cells, the viruses spread within the tumor and go on to infect other cancer cells. Distinct advantages of the virotherapy includes: (1) viruses infect and replicate in a highly tumor-selective way and thus are relatively non-pathogenic to healthy tissues; (2) viruses can utilize multiple genetic means to attack tumor cells and cause cell lysis; (3) viruses can be genetically manipulated to include additional features for improving safety and efficacy (Chiocca and Rabkin 2014). The therapy has shown promising results in preclinical tests and clinical trials for a number of tumor types (Kasuya et al. 2005; Kirn and McCormick 1996; Kirn et al. 1998; Parato et al. 2005).

Importantly, however, the tumor cell oncolysis process induces immune responses for both the viruses and the tumor: the innate immunity tends to limit virus replication and/or spread, whereas the adaptive immunity works in a manner against the tumor (Chiocca and Rabkin 2014; Melcher et al. 2011; Lawler and Chiocca 2015). Thus, the interactions of oncolytic viruses and the immune systems may contribute to therapeutic outcomes in two opposite fashions: negatively through the anti-virus immune response, and positively through the anti-tumor immune response.

Despite the promising future of the virotherapy, our knowledge in the field is still limited and several challenges remain in current clinical study (Shah et al. 2003; Lawler and Chiocca 2015; Marchini et al. 2016). For example, what is the relative

contribution of direct viral oncolysis and indirect immune suppression to the overall therapeutic efficacy? How to effectively combine the oncolysis and the virus-mediated immunity, and how to strategically manipulate the balance between anti-virus and anti-tumor immune responses? Meanwhile, genetically reprogramming the viruses so as to improve tumor cell oncolysis, while provoking robust and long-lasting anti-tumor immunity, will be particularly important for the success of the therapy (Woller et al. 2014). In addition, the mechanisms underlying tumor sensitivity and resistance under the therapy are unclear at present and demand further investigation.

Mathematical modeling, analysis, and simulation, as a power means of theoretical research, have long provided useful insight into the complications of tumor growth and the effectiveness of various tumor treatments. Such findings can offer potentially critical guidelines in the design, validation, and improvement in cancer management strategies. Recent reviews on mathematical tumor modeling can be found in Wodarz and Komarova (2005), Friedman (2007), Lowengrub et al. (2010), Araujo and McElwain (2004), and representative work in the field can be found at the references therein.

In particular, a number of mathematical studies have been devoted to the virotherapy and its impact on tumor growth. Wodarz (2001) and Novozhilov et al. (2006) proposed ordinary differential equation (ODE)-based models, with two compartments representing the infected and uninfected tumor cell populations. Each cell population is assumed to grow in a logistic fashion, and there is no separate equation for viral dynamics. Karev et al. (2006) extended these models to a more general differential equation modeling framework, with an emphasis on tumor cell heterogeneity. Tian (2011) analyzed the interaction between tumor cells and viruses, also using an ODE model, and focused on the bifurcation study of the virus replicability that is measured by the burst size. Wu et al. (2001) formulated a model using a system of partial differential equations (PDEs) and compared the evolution of a tumor under different initial conditions that resulted from three virus-injection strategies. Friedman et al. (2005) proposed a PDE-based model to investigate tumor virotherapy with host immunity. Their model, however, only considered the innate immune response and did not include the adaptive immunity.

A goal of the present paper is to establish a new mathematical and computational modeling framework for tumor virotherapy that can describe the complex interaction among tumor cells, oncolytic viruses, and immune systems, and that can incorporate both innate and adaptive immune responses. To that end, we construct a reaction–convection–diffusion system, with the motion of cells represented by a convection process and that of viruses represented by a diffusion process. The cell–virus interaction follows an 'epidemic' route: the viruses work as the pathogen that attack and infect the normal (or, susceptible) tumor cells. The infected tumor cells stimulate immune responses, both for the anti-virus innate immunity and the anti-tumor adaptive immunity. Meanwhile, new viruses are generated and spread through the lysis of the infected tumor cells and continue infecting other tumor cells. Most importantly, our model contains a moving boundary that explicitly describes the change of the tumor size with time.

The strongly nonlinear PDE system and the presence of an unknown moving boundary make our model analytically intractable. Nevertheless, using carefully designed computational methods that ensure high accuracy and robust numerical stability, we are able to conduct an extensive numerical study. In particular, we have investigated

the growth pattern of the tumor, which is a direct indication for the efficacy of the tumor therapy, under a wide range of settings that include variations of several key parameters and comparisons of tumor growth with and without delay in the adaptive immunity, as well as different types of viral dose administrations.

The remainder of this paper is organized as follows. In Sect. 2, we present details of our mathematical model, together with useful notations and necessary assumptions. In Sect. 3, we conduct numerical simulation, present representative results for a number of scenarios, and explain the biological relevance of our findings. Finally, we conclude the paper with some discussion in Sect. 4.

2 Mathematical Formulation

We first present our mathematical model that describes the interaction among tumor cells, oncolytic viruses, and immune responses, and the growth of the tumor that results from such interaction.

We consider a radially symmetric tumor. Let t denote the time and ρ denote the spatial distance measured from the center of the tumor. Let also $R(t)$ be the moving boundary of the tumor (that is changing with time). In addition, we define

$X(\rho, t)$ = number density of tumor cells not yet infected by the viruses;
$Y(\rho, t)$ = number density of tumor cells already infected by the viruses;
$Z_1(\rho, t)$ = number density of innate immune cells;
$Z_2(\rho, t)$ = number density of adaptive immune cells;
$V(\rho, t)$ = number density of viruses;
$N(\rho, t)$ = number density of dead tumor cells;
$U(\rho, t)$ = radial velocity of the tumor cells.

We assume that all the above mentioned cells have the same size and are uniformly distributed in the tumor. We also assume that the total cell density is a constant, i.e.,

$$X + Y + Z_1 + Z_2 + N = \theta = \text{Const.} \tag{1}$$

where $\theta \approx 10^6$ cells mm^{-3} (Friedman et al. 2005). For convenience of discussion, we will normalize the total cell density such that $\theta = 1$. Consequently, X, Y, Z_1, Z_2, and N become the percentages (or volume fractions) out of the constant total for their respective cell densities.

The uninfected tumor cells grow at a proliferation rate λ. Meanwhile, they are infected by the viruses (through cell–virus contact) at a rate β and subsequently enter the class of infected tumor cells. In addition, the anti-tumor adaptive immune response kills these tumor cells (through cell–cell contact) at a rate k_2 and these subsequently enter the class of dead tumor cells. In contrast, the innate immune response works against the virotherapy and kills the infected tumor cells at a rate k_1. Additionally, the infected tumor cells have a lysis rate of δ. The innate and adaptive immune cells are stimulated through their interaction with the infected tumor cells at rates of s_1 and s_2, respectively, and are cleared at rates of c_1 and c_2. The dead cells are removed at a rate μ. New viruses are produced through the lysis of the infected tumor cells

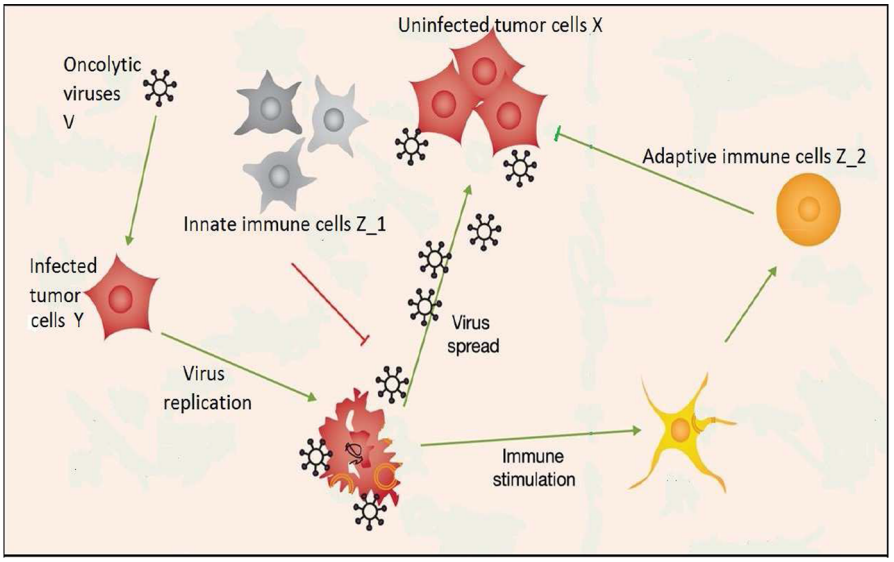

Fig. 1 (Color figure online) The interaction among oncolytic viruses, tumor cells, and immune responses [picture modified from Fig. 1 in Ref. Chiocca and Rabkin (2014)]

with a burst size b. Moreover, the viruses are cleared at a rate γ, as well as killed by the innate immune response (through cell–virus contact) at a rate k_0. Finally, we assume that all cells undergo a convection process along the radial direction of the tumor with a convection velocity U. Viruses, on the other hand, are much smaller than cells in size (typically, the diameter of a cell is 100 times larger than that of a virus) and their motion tends to be random and non-unidirectional. Thus, we assume that viruses follow a diffusion process with a diffusion rate D. A picture illustrating the virus-tumor-immune interaction is shown in Fig. 1.

These assumptions yield the following differential equations

$$\frac{\partial X}{\partial t} + \frac{1}{\rho^2}\frac{\partial}{\partial \rho}(\rho^2 U X) = \lambda X - \beta X V - k_2 X Z_2, \tag{2a}$$

$$\frac{\partial Y}{\partial t} + \frac{1}{\rho^2}\frac{\partial}{\partial \rho}(\rho^2 U Y) = \beta X V - k_1 Y Z_1 - \delta Y, \tag{2b}$$

$$\frac{\partial Z_1}{\partial t} + \frac{1}{\rho^2}\frac{\partial}{\partial \rho}(\rho^2 U Z_1) = s_1 Y Z_1 - c_1 Z_1, \tag{2c}$$

$$\frac{\partial Z_2}{\partial t} + \frac{1}{\rho^2}\frac{\partial}{\partial \rho}(\rho^2 U Z_2) = s_2 Y Z_2 - c_2 Z_2, \tag{2d}$$

$$\frac{\partial N}{\partial t} + \frac{1}{\rho^2}\frac{\partial}{\partial \rho}(\rho^2 U N) = k_1 Y Z_1 + k_2 X Z_2 + \delta Y - \mu N, \tag{2e}$$

$$\frac{\partial V}{\partial t} - D\frac{1}{\rho^2}\frac{\partial}{\partial \rho}\left(\rho^2 \frac{\partial V}{\partial \rho}\right) = b\delta Y - k_0 Z_1 V - \gamma V, \tag{2f}$$

$$\frac{1}{\rho^2}\frac{\partial}{\partial \rho}(\rho^2 U) = \lambda X + s_1 Y Z_1 + s_2 Y Z_2 - c_1 Z_1 - c_2 Z_2 - \mu N. \tag{2g}$$

Here the last equation is obtained by adding up the first five equations and using the fact that the total cell density is a constant. These equations hold on the spherical domain $0 \leq \rho \leq R(t)$ for $t \geq 0$. Meanwhile, the free boundary, $R(t)$, satisfies the kinematic condition,

$$\frac{\mathrm{d}R}{\mathrm{d}t} = U(R(t), t). \tag{3}$$

Boundary and initial conditions are necessary to complete the model. In particular, we need to prescribe the boundary conditions for V, which is governed by a parabolic equation, and U, which satisfies an ordinary differential equation. We consider the ideal situation that all the free viruses remain in the tumor and impose a homogeneous Neumann condition for V at the tumor boundary:

$$\frac{\partial V}{\partial \rho}(R(t), t) = 0. \tag{4a}$$

At the tumor center, the spherical symmetry implies that

$$U(0, t) = 0, \tag{4b}$$

$$\frac{\partial V}{\partial \rho}(0, t) = 0. \tag{4c}$$

3 Results

Mathematical analysis of the system (2) is challenging since it is strongly nonlinear with mixed types of PDEs. Meanwhile, the presence of an unknown moving boundary adds more difficulty. Instead, we have chosen to utilize numerical simulation in order to gain useful biological insight. Details of our numerical algorithms are provided in "Appendix A". Essentially, we map the original spatial domain with a moving boundary, $0 \leq \rho \leq R(t)$, into a fixed domain, $0 \leq r \leq 1$, through a time-dependent coordinate transformation, which enables us to design and implement numerical methods of second-order accuracy and robust stability.

Using such algorithms, we have conducted extensive numerical simulation to our model. We then present the simulation results throughout this section with detailed explanations. The base values of the model parameters used in our simulation are listed in Table 1. Most of these parameter values are taken from the literature but with necessary adjustments to be consistent with our normalized variables. In particular, the value of the burst size b in our study is rescaled from that in Wang and Tian (2008), Friedman et al. (2005)—the base value $b = 1$ here corresponds to a realistic viral burst size of 50, for the oncolytic virus hrR3 (Fulci et al. 2006). Meanwhile, the values of the tumor proliferation rate λ, the viral infection rate β, the lysis rate δ, the take-up rate k_0, and the removal rates γ and μ are obtained based on experimental observations in Fulci et al. (2006), Pecora et al. (2002). The diffusion coefficient D is calculated approximately using the Einstein formula (Chaplain et al. 1998). Additionally, the killing rate k_1, the stimulation rate s_1, and the clearance rate c_1 for the innate immune

Table 1 Parameters and baseline values

Symbol	Description	Value
λ	Proliferation rate of tumor cells	$2.0\,\mathrm{h}^{-1}$
β	Viral infection rate	$3.5\,\mathrm{mm}^3\,\mathrm{h}^{-1}\,\mathrm{virus}^{-1}$
k_1	Innate immune killing rate	$2.0\,\mathrm{mm}^3\,\mathrm{h}^{-1}\,\mathrm{cell}^{-1}$
k_2	Adaptive immune killing rate	$2.0\,\mathrm{mm}^3\,\mathrm{h}^{-1}\,\mathrm{cell}^{-1}$
s_1	Innate immunity stimulation rate	$56.0\,\mathrm{mm}^3\,\mathrm{h}^{-1}\,\mathrm{cell}^{-1}$
s_2	Adaptive immunity stimulation rate	$56.0\,\mathrm{mm}^3\,\mathrm{h}^{-1}\,\mathrm{cell}^{-1}$
c_1	Clearance rate of innate immune cells	$2.0\,\mathrm{h}^{-1}$
c_2	Clearance rate of adaptive immune cells	$2.0\,\mathrm{h}^{-1}$
D	Diffusion coefficient of viruses	$3.6\,\mathrm{mm}^2\,\mathrm{h}^{-1}$
δ	Infected cell lysis rate	$5.6\,\mathrm{h}^{-1}$
k_0	Take-up rate of viruses by innate immunity	$1.0\,\mathrm{mm}^3\,\mathrm{h}^{-1}\,\mathrm{cell}^{-1}$
γ	Clearance rate of viruses	$2.5\,\mathrm{h}^{-1}$
μ	Removal rate of dead cells	$2.1\,\mathrm{h}^{-1}$
b	Viral burst size	$1.0\,\mathrm{virus\,cell}^{-1}$

response are estimated in Friedman et al. (2005). We have not found any relevant data to quantify the characteristics of the adaptive immune response in tumor growth. Hence, in this study we have assumed that the killing rate k_2, the stimulation rate s_2 and the clearance rate c_2 for the adaptive immunity take the same base values as those for the innate immunity.

We use the same initial conditions as given in Friedman et al. (2005), which are based on laboratory experiments conducted on rats with brain tumors. (For completeness, we list these initial conditions in "Appendix A"). The tumor size is initialized as $R(0) = 2$ mm, at which time the oncolytic viruses are injected into the center of the tumor and the process of virotherapy starts. A Gaussian distribution is used to represent the initial profile of the viruses inside the tumor.

Throughout the numerical simulation, we focus our attention on the change of the tumor size with respect to time. The tumor size is a crucial factor in the measurement of the degree of cancer and the efficacy of a therapy; continual growth of a tumor is typically an indication of the malignancy (and progressive worsening) of the tumor. (As reported in Fulci et al. (2006) for the experiments on rats, when the brain tumor grows to a size with 6 mm in radius, it usually kills a rat). Thus, in our numerical study, we will especially examine the time evolution of the tumor boundary $R(t)$, which directly measures the size of the tumor, to help us understand the effects of the virotherapy.

3.1 Baseline Solutions

Figure 2 displays the change of $R(t)$ with respect to time under the virotherapy, using parameter values described in Table 1, referred to as the base values. We observe that the tumor grows almost linearly for the first 50 h, due to the fact that the viruses are

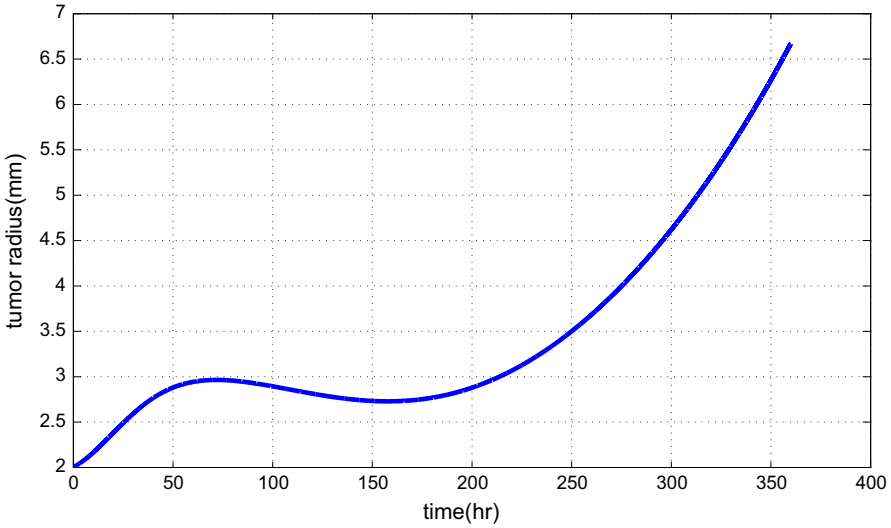

Fig. 2 (Color figure online) Change of tumor radius with time

injected into the center of the tumor and it takes time for the viruses to spread, to interact with the tumor cells, and to stimulate immune response throughout the tumor. Thus, the efficacy of the therapy is not fully reflected in this initial period. During the next 150 h or so, however, the tumor completely stops growing and even decays slightly, indicating that the virotherapy is taking effect. Finally, the tumor starts to regrow after the effective period of the treatment. Despite the re-growth of the tumor, the contribution of the therapy is clear: it has suppressed the tumor growth for a significant period of time (around 150 h).

Figure 3 shows the profiles of the densities for the uninfected tumor cells (X), the innate immune cells (Z_1) and the adaptive immune cells (Z_2) at several times during this process, under the same setting as in Fig. 2. The uninfected tumor cells are initially set at 80% with a uniform distribution on the transformed spatial domain, $0 \leq r \leq 1$ (see Fig. 3a). At $t = 100$ h, their density has been reduced to a much lower level, ranging between 9 and 20%, due to the interaction with the oncolytic viruses. The reduction is most significant for the region near the center of the domain ($r = 0$), where the viruses have the highest concentration. We also note that the time falls within the period of non-growth of the tumor in Fig. 2. When $t = 200$ h, however, X has increased to a level of 45–65% (again the lowest density occurs near the center); correspondingly, we see from Fig. 2 that the tumor has started to regrow. As time goes on, X continues increasing and, at $t = 360$ h, it is already close to 100%. On the other hand, the densities of the immune cells, Z_1 and Z_2 , show an opposite trend (see Fig. 3b, c). They are initially set as 5% uniformly for each and then increase owing to the stimulation of the infected tumor cells. At $t = 100$ h, Z_1 reaches a level ranging between 30 and 40%, with the highest density occurring near the center of the domain, whereas Z_2 ranges between 12 and 20%, with the highest density near the boundary of the domain. Afterward the densities of the immune cells start decreasing and, at

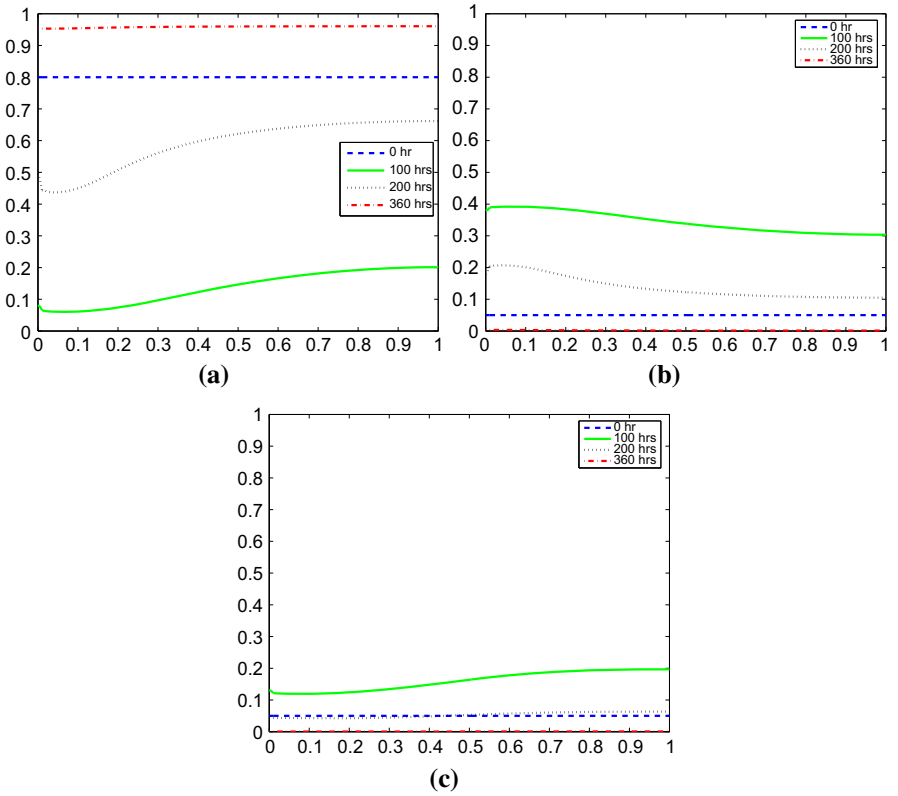

Fig. 3 (Color figure online) Distribution of uninfected tumor cells and immune cells at different times, **a** uninfected tumor cells, **b** innate immune cells, **c** adaptive immune cells

$t = 360$ h, both Z_1 and Z_2 are almost 0%. These are consistent with the pattern of the tumor growth exhibited in Fig. 2.

3.2 Effects of Parameter Variation

Naturally, we hope to improve the baseline result presented in Figs. 2 and 3. To that end, it is necessary that we understand, and quantify, the contribution of the various parameters that appear in the model (2). Hence, we proceed to analyze the effects of the variation of a few key parameters and conditions on the growth of the tumor.

Figure 4 displays the results of varying the two immune killing rates: k_1 for the innate immunity and k_2 for the adaptive immunity. As we know, the innate immune response works in an anti-viral manner, whereas the adaptive immune response tends to be anti-tumor. Figure 4 shows that when fixing $k_2 = 2$ at its base value and increasing k_1 from its base value to 20, the tumor would grow faster than its baseline scenario after an initial transient period. In contrast, when fixing $k_1 = 2$ at the base value and increasing k_2 to 20, the tumor would grow slower, and eventually decay in size,

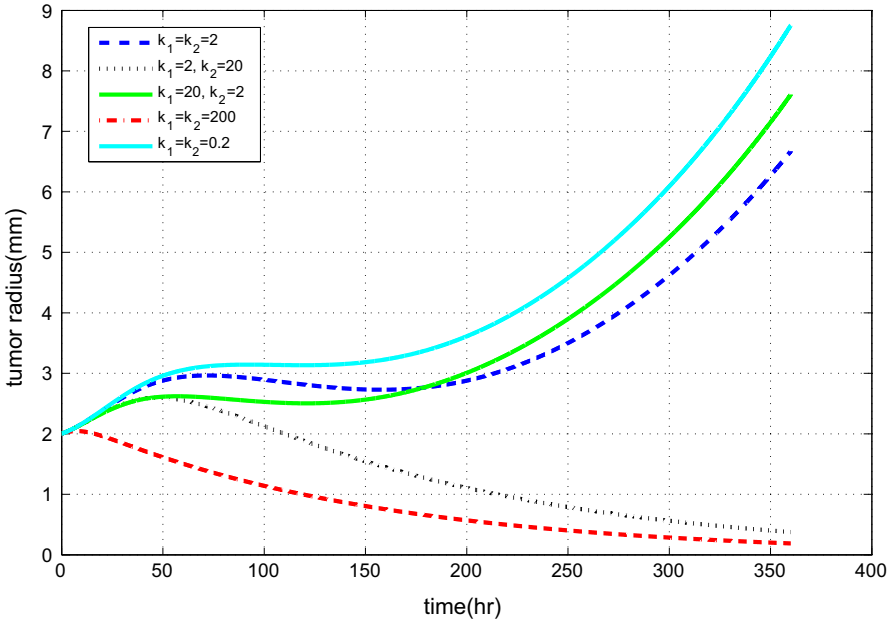

Fig. 4 (Color figure online) Tumor growth with different immune killing rates

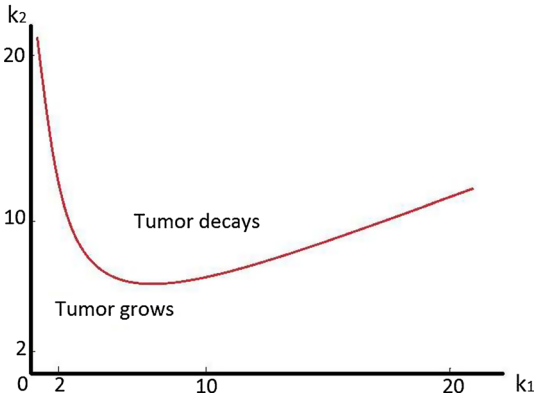

Fig. 5 (Color figure online) A bifurcation diagram for tumor growth with respect to the two immune killing rates

demonstrating a higher level of anti-tumor effect with the increased adaptive immunity. In addition, when k_1 and k_2 are both decreased to a small value, 0.2, the tumor would grow significantly faster; when both parameters are at a large value, 200, the tumor would decay from the very beginning, implying that immune responses are necessary for the success of the virotherapy. To gain more insight into the effects of the two immune killing rates on tumor growth, we have created a bifurcation diagram in the (k_1, k_2) plane, shown in Fig. 5. The red curve in Fig. 5 displays the boundary that separates two parameter regions, i.e., the tumor grows in one region and decays in the other.

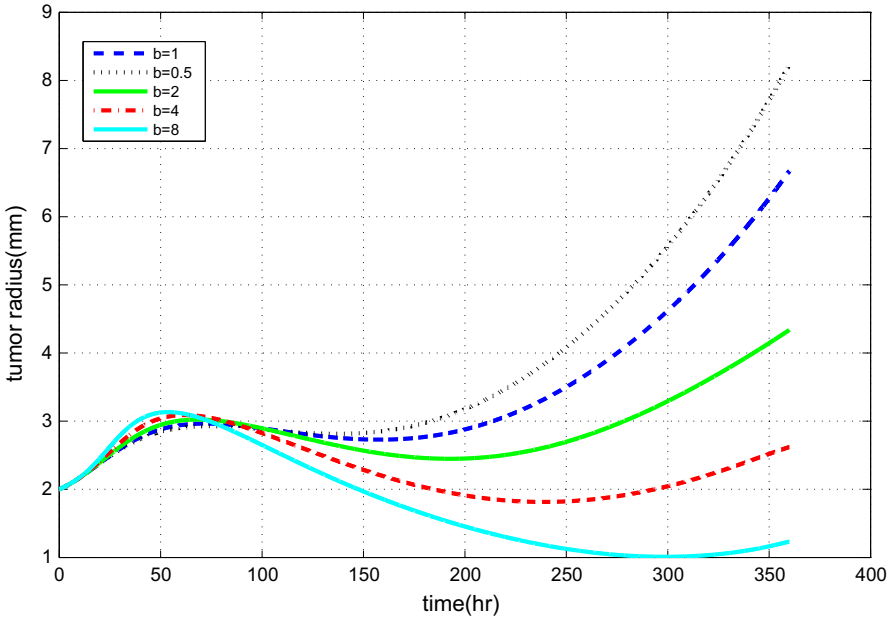

Fig. 6 (Color figure online) Tumor growth with different values of viral burst size

Next, we perform a study on the viral burst size, b, representing the number of new viruses coming out from a lysis of an infected tumor cell. The burst size is a direct measurement of the replicability of the viruses and is expected to play an important role in the virotherapy. With higher values of b, new viruses are generated faster which could promote the efficacy of the therapy. Figure 6 shows the growth of the tumor with respect to several different values of b, while fixing all other parameters at their base values. The pattern is clear: when b decreases, the tumor grows faster; when b increases, the growth of the tumor slows down. In particular, with a relatively big value $b = 8$, the tumor decreases in size for a period as long as 250 h ($50 \leq t \leq 300$), before it starts re-growing.

In addition, we are interested in explicitly assessing the contribution from each of the two types of immune responses. We do this through comparing the baseline solution with two hypothetical (and extreme) cases: (1) only the innate immunity is present; (2) only the adaptive immunity is present. As can be observed from the system (2), if $Z_1 = 0$ at $t = 0$, then Z_1 would stay at 0 for all the time. The same is true for Z_2 . Thus, we may remove one type of immunity from the model, while retaining the other, by changing the initial conditions. Figure 7 shows several scenarios along this line. We see that for the two cases where the adaptive immunity is absent ($Z_2 = 0$), the tumor grows faster in comparison with the baseline growth curve, and the one with higher initial value of Z_1 outcompetes the other. In contrast, for the two cases where the innate immunity is absent ($Z_1 = 0$), the tumor grows slower and has a much longer non-growth period, than that for the baseline curve.

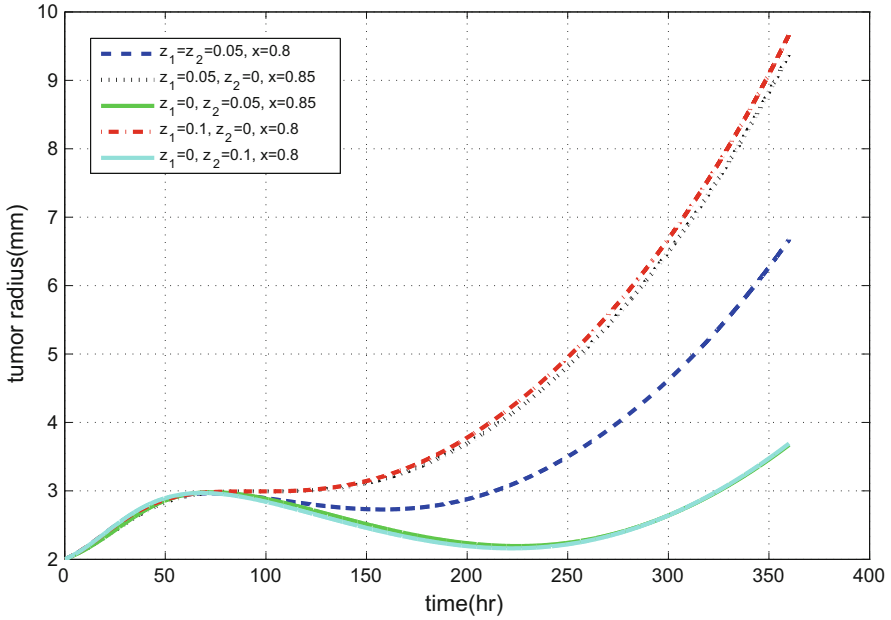

Fig. 7 (Color figure online) Impact of the two immune systems on tumor growth, where x, z_1 and z_2 denote the initial profiles of X, Z_1 and Z_2, respectively

3.3 Effects of Delayed Adaptive Immunity

In the model (2), we have assumed that the two types of immune responses, innate and adaptive, would be stimulated simultaneously and get started at the same time. In reality, however, it is observed that although the innate immune response is fast and can be treated as instantaneous, the adaptive immune response is typically on a slower pace; it may take a time frame ranging from several hours to a few days to activate the adaptive immune system after the viruses are injected into, and start interacting with, the tumor (Lawler and Chiocca 2015; Melcher et al. 2011). Thus, there could be a gap between the starting times of the two immune responses, and such non-synchronization may have additional impact on the efficacy of the virotherapy.

To investigate this issue, we introduce a time delay to our equation for the adaptive immunity (Z_2). Thus, Eq. (2d) becomes

$$\frac{\partial Z_2}{\partial t} + \frac{1}{\rho^2}\frac{\partial}{\partial \rho}(\rho^2 U Z_2) = s_2 Y(\rho, t-T) Z_2(\rho, t-T) - c_2 Z_2\,, \tag{5}$$

where T is a constant that represents the delay in the stimulation of the adaptive immune response. Consequently, Eq. (2g) will be replaced by

$$\frac{1}{\rho^2}\frac{\partial}{\partial \rho}(\rho^2 U) = \lambda X + s_1 Y Z_1 + s_2 Y(\rho, t-T) Z_2(\rho, t-T) - c_1 Z_1 - c_2 Z_2 - \mu N\,. \tag{6}$$

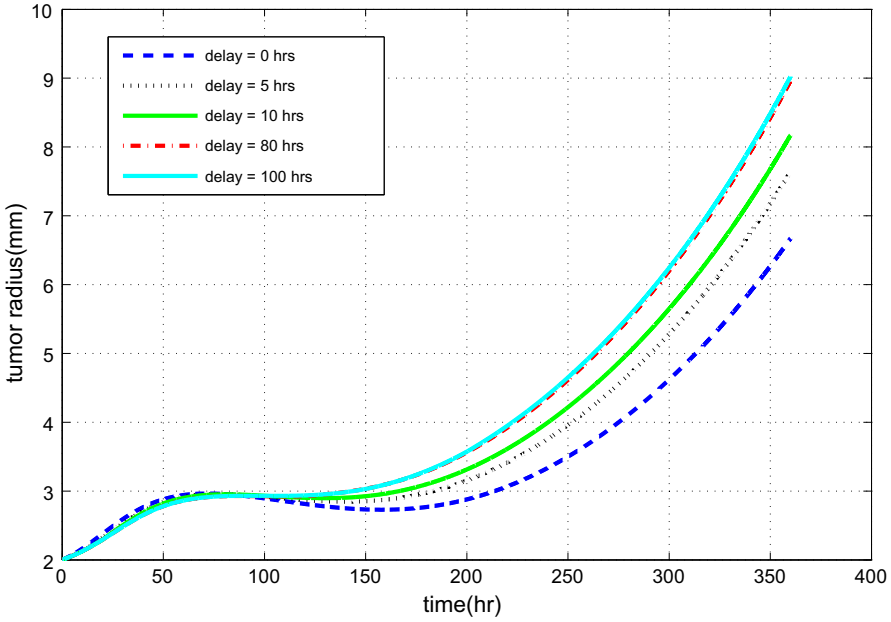

Fig. 8 (Color figure online) Tumor growth with and without delay in the adaptive immune response

Other equations in the system (2) will remain the same.

The numerical methods described in "Appendix A" can be applied, with minor modification, to compute our tumor model with the time delay. Results are presented below.

Figure 8 shows the comparison for the growth of the tumor without delay ($T = 0$) and with several different delays ($T = 5,\ 10,\ 80,\ 100$ h), using the baseline parameter values given in Table 1. For the first 100 h or so, there is little difference among the five cases, as the cell–virus interaction is in the initial phase of adjustment and the tumor is still growing for most of this initial period. The difference becomes apparent later on, especially when the tumor starts re-growing after the non-growth period ($t > 200$). It appears that the re-growth rate increases with T; the case with the largest delay ($T = 100$ h) grows the fastest among the five, though the two curves with $T = 80$ and $T = 100$ almost coincide with each other. An implication is that a delayed start of the adaptive immune response would not significantly impact the virotherapy in the short term, i.e., the first few days, when the therapy is not yet, or just starts being, fully effective. Instead, the delayed adaptive immunity would make a difference for the longer-term development of the tumor, in a negative way: the more delayed (up to $T = 100$ h), the faster the tumor regrows.

With the delayed adaptive immunity, we have also performed a study on the variation of a few key model parameters, and we observe similar patterns as shown in Fig. 4 for different immune killing rates, Fig. 6 for different burst sizes, as well as Fig. 7 for different initializations of the two immune responses. For illustration, Fig. 9 compares the two cases of $T = 0$ (without delay) and $T = 5$ h (with delay) for two sets of

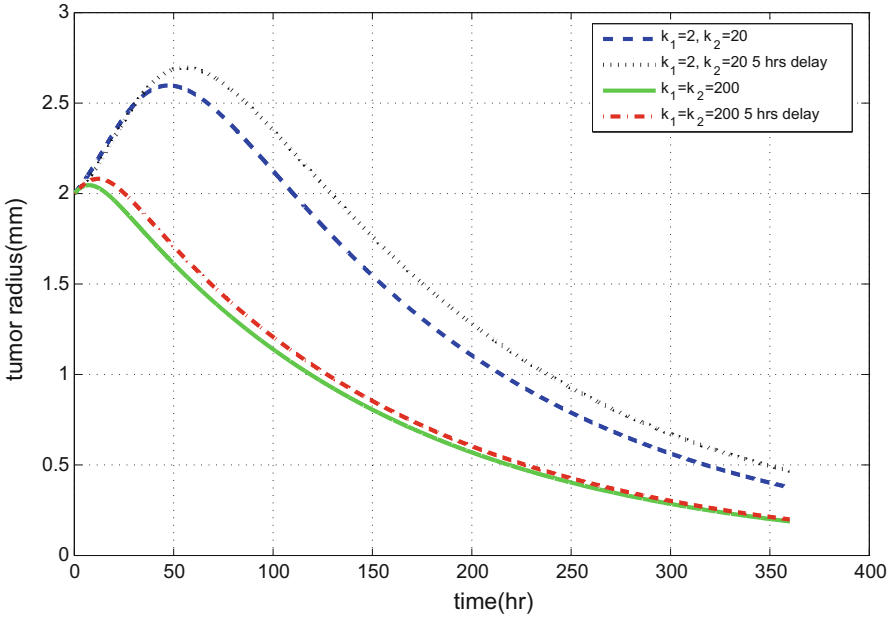

Fig. 9 (Color figure online) Tumor growth with and without delay for two different sets of immune killing rates

hypothetical values of the immune killing rates. For each set of values for k_1 and k_2, the anti-tumor immune effects have been strong enough so that the tumor radius would quickly decrease immediately after the initial growth, and there is no re-growth happening. For each case, however, there is a difference between the scenario of no delay and that of 5 h delay: the curve with $T = 5$ is above the one with $T = 0$, showing a slower decay rate. The difference is only apparent during the decay phase of the tumor and is not noticeable during the initial growth period. Meanwhile, Fig. 10 shows two choices of the burst size for the cases $T = 0$ and $T = 5$, while other model parameters are fixed at their base values. For each choice of b, the tumor development exhibits three phases: initial growth, non-growth (decay), and re-growth. The two curves $T = 0$ and $T = 5$, for each b, almost coincide with each other during the first two phases, but only move away from each other during the re-growth phase; the one with delay regrows faster than the other. In all these results, a delayed adaptive immunity appears to have a negative impact on the efficacy of the virotherapy, but only for the longer-term development of the tumor.

In addition, we remark that our model provides an explicit means to represent the delay of the adaptive immune response. Alternatively, such a delay may be incorporated in an implicit manner. For example, if we assume that the innate immune response plays a role in triggering the adaptive immune response [see more discussion in Parish and O'Neill (1997)], we may modify the right-hand side of Eq. (5) by $s_2 Y Z_1 Z_2 - c_2 Z_2$, without explicit dependence on the delay T. We have found through our numerical simulation that such an implicit approach could reproduce some of the results shown here for our explicit delay model.

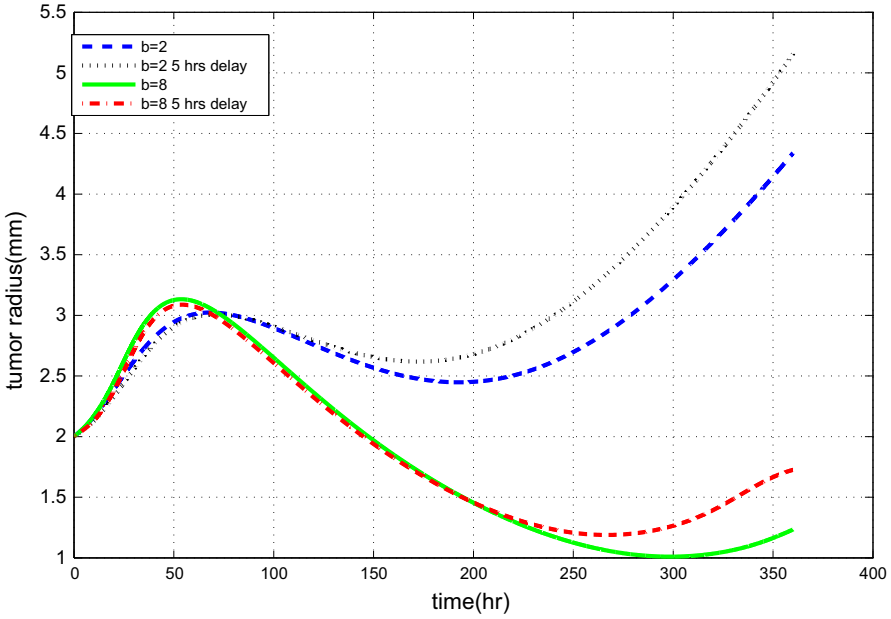

Fig. 10 (Color figure online) Tumor growth with and without delay for two different choices of viral burst size

3.4 Effects of Large Burst Size

It has been shown that the viral burst size, b, plays an important role in the process of virotherapy. In particular, increased efficacy of the therapy has been observed with higher values of b (see Figs. 6, 10). Biomedically, the oncolytic viruses can be engineered so as to produce different burst sizes, possibly at large values. For example, Kambara et al. (2005) reported a new glioma-specific virus (herpes simplex virus type 1 mutant) with a high replication capability that led to significantly increased survivals of animals (mice) with brain tumors. Additionally, it is known that for some wild-type herpes simplex viruses, the burst size ranges in the thousands (Friedman et al. 2005). Thus, a natural question in our study is to explore the consequence of large burst size (hence high replicability) regarding the tumor development, in the complex interaction among tumor cells, viruses, and immune responses, and even with delayed adaptive immunity.

As shown in Fig. 6, when increasing the value of b slightly above its baseline value, the length of the non-growth period is increased, though the tumor would eventually regrow. Additional numerical investigation reveals that when b gets even larger, the efficacy will be further increased: when $b \geq 10$, the tumor will eventually shrink to a level almost at 0, after several cycles of decay and re-growth; when $b \geq 50$, there will be no re-growth taking place for the tumor. Figure 11 illustrates the situations with three larger burst sizes: 10, 25, 100. For $b = 10$ and 25, we still observe some re-growth trends, but all happening after $t = 300$ h. For $b = 100$, the tumor development only exhibits two phases: an initial growth, followed by a quick decay to a size very close

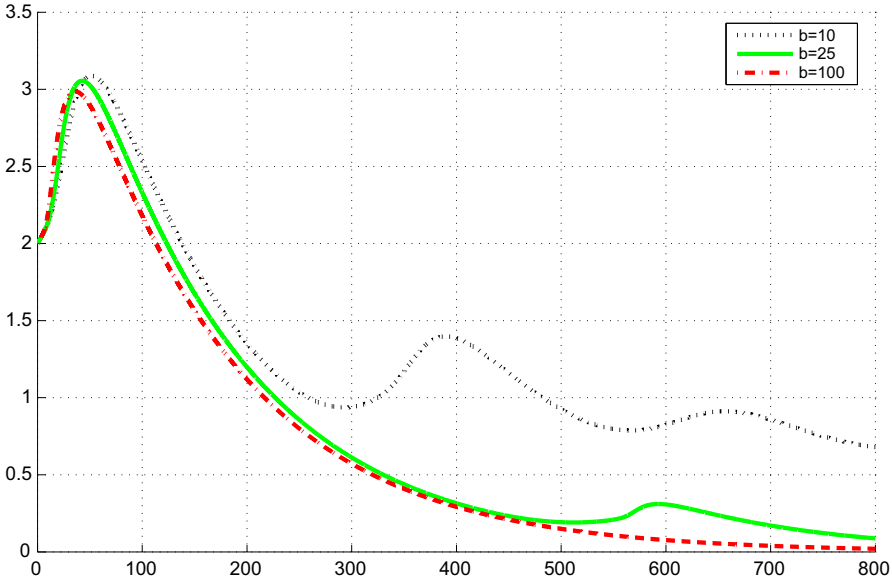

Fig. 11 (Color figure online) Tumor growth with large values of viral burst size

to 0 at $t \approx 700$. Once approaching there, the tumor size remains at that extremely low level for all the time $t > 700$, indicating that the tumor has essentially been eliminated.

Figure 12 shows the time evolution of the distributions for the uninfected tumor cells and the two types of immune cells, with the same initial settings as those in Fig. 3, but with a large burst size $b = 100$. In contrast to the results in Fig. 3, we now observe that X keeps decreasing and, at $t = 12.5$ h, the value of X is already very close to 0. Though not shown here, X will stay at that level for all the later times, an indication of the success of the therapy. Meanwhile, the values of Z_1 and Z_2 keep increasing and eventually reach the levels around 65 and 15%, respectively, due to the continuing stimulation of the viruses and infected tumor cells. These are consistent with the tumor growth pattern shown in Fig. 11.

3.5 Effects of Repeated Virus Injection

Our study so far has focused on the case with a single virus injection which is administered in the beginning of the treatment ($t = 0$). In a recent virotherapy clinical trial (Andtbacka et al. 2015), a virus dose was administered (via intratumoral injection) every 2 weeks to several hundreds of patients with skin cancer and the outcomes were encouraging, with demonstrated therapeutic benefit for patients with metastatic tumors. This result suggests the importance of continuing treatment through repeated virus injection.

We proceed to numerically test this scenario by re-setting the virus distribution to its initial configuration (see Eq. 10b) in every 2 weeks, or 336 h. This represents a biweekly injection of viruses into the tumor center. Other conditions and parameters

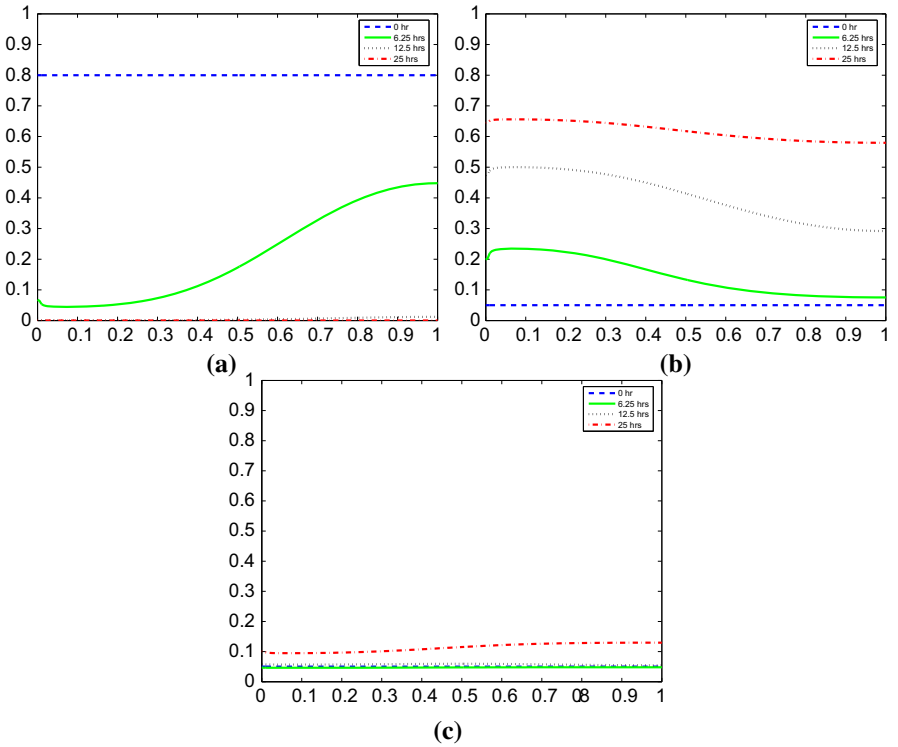

Fig. 12 (Color figure online) Distribution of uninfected tumor cells and immune cells at different times with a large burst size $b = 100$, **a** uninfected tumor cells, **b** innate immune cells, **c** adaptive immune cells

are kept at their default (or, baseline) values. Figure 13 compares the tumor growth with such a biweekly virus injection and with a single virus injection (at $t = 0$), where $b = 1,\ 10$ and 100, respectively. For the first two cases, the improvement in efficacy with the repeated virus doses is evident; particularly, for $b = 10$, the tumor shrinks much faster than that with a single virus dose in the beginning. For the third case, $b = 100$, the two types of virus administrations do not make any difference, as the viral burst size has been large enough so that only a single virus dose is needed to quickly control (and conquer) the tumor.

4 Discussion

We have presented a new mathematical model for tumor virotherapy with virus-mediated immune responses. The model is a system of PDEs that couples tumor growth with cell–virus–immune interactions and that describes the motion of tumor cells and viruses on a domain with a moving boundary. A distinctive feature of our model is the incorporation of both innate and adaptive immune responses in the course of tumor oncolysis, which, to our knowledge, has not been investigated in prior mathematical models and studies. The modeling framework and the computational methods

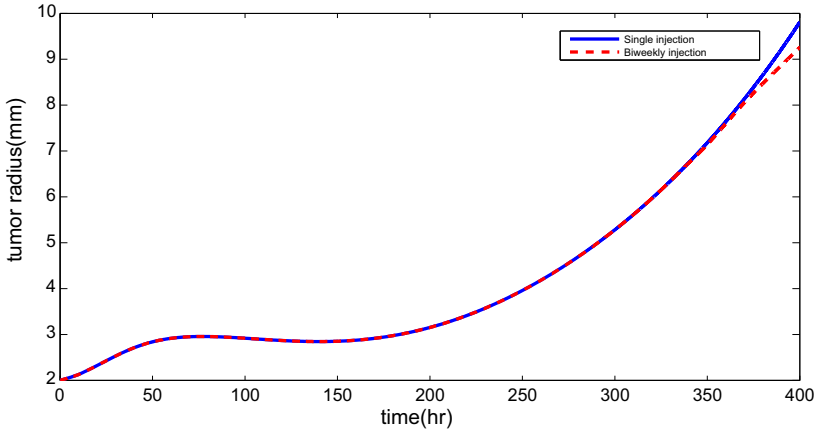

(a)

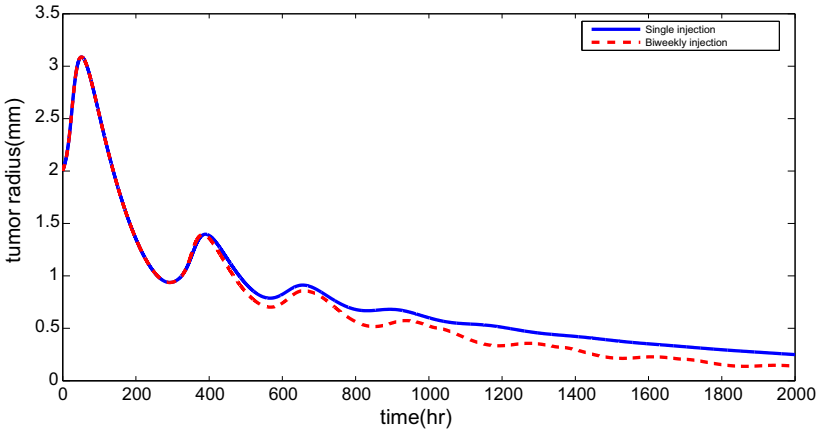

(b)

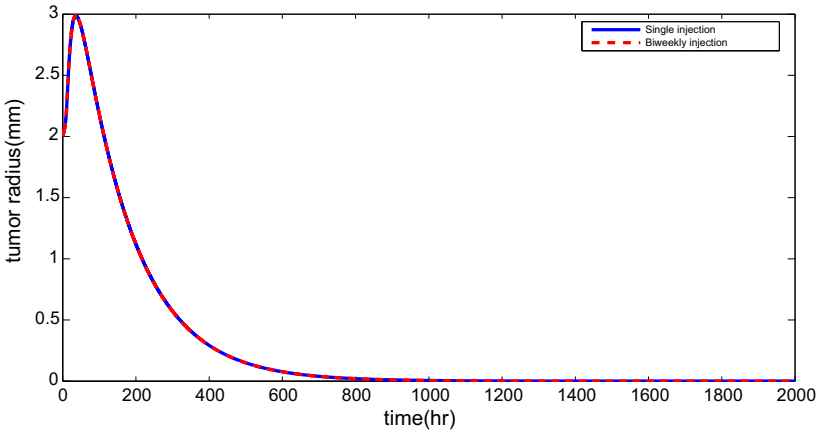

(c)

Fig. 13 (Color figure online) Tumor growth with single virus injection and repeated biweekly virus injection, using different values of viral burst size, **a** $b = 1$, **b** $b = 10$, **c** $b = 100$

presented in this paper allow us to conduct a novel and careful study on tumor dynamics under the virotherapy, in a wide range of settings that include varied parameters and initial conditions, delay in the adaptive immunity, and repeated viral doses.

Our results show that a typical scenario of tumor evolution under the virotherapy may exhibit three phases: initial growth, non-growth or even shrinking in size (which may correspond to a period of cancer dormancy), and re-growth (representing cancer recurrence). We have found, however, when the adaptive immune killing rate and/or the viral burst size are increased, the efficacy of the therapy is significantly improved. Particularly, with sufficiently large values for these parameters, tumor re-growth will not occur and the tumor will shrink to, and stabilize at, a size very close to 0. The findings suggest that genetically manipulating oncolytic viruses so as to promote the anti-tumor adaptive immunity and the viral replicability, would be potentially useful means to enhance the efficacy of the virotherapy. In addition, our results demonstrate that repeated administration of viral doses on regular intervals (e.g., 2 weeks) leads to improved efficacy, which is consistent with the clinical observation.

The presence of two different types of immune responses and their coupling with tumor growth and host–virus interaction are an emphasis of this work. We find that the immune responses are necessary for the success of the virotherapy. The ideal therapeutic outcome, i.e., removal of both the tumor and viruses can be possibly achieved through genetically engineered viruses with enhanced oncolytic capability and through a right combination of the virus-mediated innate and adaptive immune responses, particularly represented by the sizes of the two immune killing rates. A delay in the start of the adaptive immune response may not have a notable effect on the short-term dynamics of tumor growth, but may negatively impact the efficacy of the virotherapy in the longer-term, especially during the tumor re-growth phase.

The findings in this study can help us better understand the complications in tumor–viral dynamics and can provide useful guidelines to design and improve the virotherapy. A limitation in our model is the relatively simple geometry; the assumption of spherical symmetry, though mathematically natural and computationally efficient, may not be able to reflect the realistic, often irregular, shapes of many tumors, and the related intricacy in tumor growth. Our modeling framework can be extended to three-dimensional spatial domain for a more general investigation of tumor growth, though with a higher level of computational challenge. We also hope to utilize clinical data to fit and validate our general mathematical formulation. Another limitation in our study is the assumption of homogeneity among all tumor cells. Practically, tumor cells may exhibit spatial heterogeneity that involves different levels of susceptibility and resistance to viral infection, varied strength of immune responses, and anisotropic movement of tumor cells and viruses. Incorporation of such heterogeneity into the modeling framework will potentially lead to deeper insight into tumor dynamics under the virotherapy.

Acknowledgements JPT and JW acknowledge partial support from the National Science Foundation under Grant Nos. 1216907 and 1216936, respectively. The authors would like to thank the anonymous referees for helpful comments which led to an improvement in this paper.

Appendix A: Numerical Methods

A difficulty in the design of numerical algorithms for the model (2) is the presence of a moving boundary, $R(t)$, which describes the growth of the tumor with time and which has to be determined as part of the solution. To partially overcome this challenge, we choose to map the original domain with the moving boundary into a fixed domain, by introducing a new coordinate:

$$r = \frac{\rho}{R(t)}\,. \tag{7}$$

Obviously, Eq. (7) transforms the original domain, $0 \le \rho \le R(t)$, into a regular interval, $0 \le r \le 1$. Based on such a mapping, we are able to develop accurate and robust numerical methods.

Equation (1) enables us to drop one variable, N. Using the change of coordinates, the original equations in (2) can be written as

$$\frac{\partial X}{\partial t} + \frac{U - rR'}{R}\frac{\partial X}{\partial r} = F_1, \tag{8a}$$

$$\frac{\partial Y}{\partial t} + \frac{U - rR'}{R}\frac{\partial Y}{\partial r} = F_2, \tag{8b}$$

$$\frac{\partial Z_1}{\partial t} + \frac{U - rR'}{R}\frac{\partial Z_1}{\partial r} = F_{3a}, \tag{8c}$$

$$\frac{\partial Z_2}{\partial t} + \frac{U - rR'}{R}\frac{\partial Z_2}{\partial r} = F_{3b}, \tag{8d}$$

$$\frac{\partial V}{\partial t} - \Big(\frac{rR'}{R} + \frac{2D}{R^2 r}\Big)\frac{\partial V}{\partial r} - \frac{D}{R^2}\frac{\partial^2 V}{\partial r^2} = F_4, \tag{8e}$$

$$\frac{1}{Rr^2}\frac{\partial}{\partial \rho}(r^2 U) = F_5, \tag{8f}$$

for $0 \leqslant r \leqslant 1$ and $t > 0$, where $R' = \frac{\mathrm{d}R}{\mathrm{d}t}$. The terms on the right-hand sides are:

$$\begin{aligned}
F_1 &= \lambda X - \beta X V - k_2 X Z_2 - F X,\\
F_2 &= \beta X V - k_1 Y Z_1 - \delta Y - F Y,\\
F_{3a} &= s_1 Y Z_1 - c_1 Z_1 - F Z_1,\\
F_{3b} &= s_2 Y(t) Z_2(t) - c_2 Z_2 - F Z_2,\\
F_4 &= b\delta Y - k_0 Z_1 V - \gamma V,\\
F_5 &= F,
\end{aligned}$$

where

$$F = \lambda X + s_1 Y Z_1 + s_2 Y(t) Z_2(t) - c_1 Z_1 - c_2 Z_2 - \mu(1 - X - Y - Z_1 - Z_2).$$

The kinematic condition in Eq. (3) and boundary conditions in Eq. (4) become

$$\frac{\mathrm{d}R}{\mathrm{d}t}(t) = U(1,t), \tag{9a}$$

$$\frac{\partial V}{\partial r}(1,t) = 0, \tag{9b}$$

$$U(0,t) = 0, \tag{9c}$$

$$\frac{\partial V}{\partial r}(0,t) = 0. \tag{9d}$$

The initial conditions are given below. In particular, the initial values for R and V are taken from Friedman et al. (2005), based on laboratory experiments conducted on rats with brain tumors. When the virotherapy starts, the oncolytic viruses are injected into the center of the tumor, which is measured at 2 mm at that time. Meanwhile, a Gaussian distribution centered at 0 is used to represent the initial profile of the viruses inside the tumor. Additionally, we note that all the cell densities have been normalized so that the total is $\theta = 1\,\text{cell mm}^{-3}$.

$$R(0) = 2\,\text{mm}\,, \tag{10a}$$

$$V(r,0) = \alpha e^{-\frac{4r^2}{a^2}}, \quad \text{where} \quad \alpha \int_0^1 \mathrm{r}^2 \mathrm{e}^{-\frac{4\mathrm{r}^2}{\mathrm{a}^2}}\,\mathrm{dr} = 0.45, \tag{10b}$$

$$X(r,0) = 0.8\,\text{cell mm}^{-3}, \quad \mathrm{Y(r,0)} = 0.1\,\text{cell mm}^{-3}, \tag{10c}$$

$$Z_1(r,0) = 0.05\,\text{cell mm}^{-3}, \quad \mathrm{Z_2(r,0)} = 0.05\,\text{cell mm}^{-3}. \tag{10d}$$

The numerical simulation of Eq. (8) is essentially a time marching problem. We denote the numerical solution at the nth time step by

$$\left(R^n, X^n, Y^n, Z_1^n, Z_2^n, U^n, V^n\right).$$

We use the second-order Adams–Bashforth method to advance R in time. Applying it to Eq. (10a) yields

$$R^{n+1} = R^n + \frac{\Delta t}{2}(3U^n - U^{n-1}). \tag{11}$$

The hyperbolic type equations, for example Eq. (8a), is solved by a leapfrog scheme:

$$\frac{X_j^{n+1} - X_j^{n-1}}{2\Delta t} + A_j^n \frac{X_{j+1}^n - X_{j-1}^n}{2\Delta r} = (F_1)_j^n, \tag{12a}$$

where

$$A = \frac{U - rR'}{R}\,, \tag{12b}$$

and the subscript j refers to the jth spatial grid point in the radial direction. Meanwhile, we supplement the leapfrog method with a simple average in time: $X_j^n = \frac{1}{2}(X_j^{n+1} +$

X_j^{n-1}), implemented in our code for every 10 steps. This additional time-average procedure is introduced to overcome potential mesh drifting instability (Press et al. 1996) when applying the leapfrog method to nonlinear equations, yet retaining its second-order accuracy (Wang and Tian 2008). In addition, Y, Z_1, and Z_2 are updated in a similar way.

Once we have X^{n+1}, Y^{n+1}, Z_1^{n+1} and Z_2^{n+1} calculated, we compute U^{n+1} using the Trapezoidal Rule for Eq. (8f):

$$r_{j+1}^2 U_{j+1}^{n+1} - r_j^2 U_j^{n+1} = \frac{R^{n+1}}{2} \Delta r \left(r_{j+1}^2 (F_5)_{j+1}^{n+1} + r_j^2 (F_5)_j^{n+1} \right). \tag{13}$$

Finally, we solve the parabolic Eq. (8e). For convenience, we write the equation in the following form:

$$\frac{\partial V}{\partial t} + A_1 \frac{\partial V}{\partial r} + A_2 \frac{\partial^2 V}{\partial r^2} = F_4, \tag{14a}$$

with

$$A_1 = -\left(\frac{r R'}{R} + \frac{2D}{R^2 r} \right) \quad , \quad A_2 = -\frac{D}{R^2}. \tag{14b}$$

Since F_4 is a linear function of V^{n+1}, the above equation is a linear parabolic equation at time step $n+1$. We use the second-order Backward Difference Formula (BDF) in time and central differences in space to approximate Eq. (14a):

$$\begin{aligned} &\frac{3V_j^{n+1} - 4V_j^n + V_j^{n-1}}{2\Delta t} + (A_1)_j^{n+1} \frac{V_{j+1}^{n+1} - V_{j-1}^{n+1}}{2\Delta r} \\ &+ (A_2)_j^{n+1} \frac{V_{j+1}^{n+1} - 2V_j^{n+1} + V_{j-1}^{n+1}}{(\Delta r)^2} = (F_4)_j^{n+1}. \end{aligned} \tag{15}$$

The discretized equation can then be written in a tridiagonal algebraic form which can be computed efficiently (Golub and Loan 2012). Once solved, a full cycle of the time marching is completed, and the procedure repeats at the next cycle.

The methods presented here achieve second-order accuracy in both time and space and possess strong numerical stability, which allows us to conduct a careful numerical study on the complex interaction among the tumor, the viruses, and the immune systems involved in the tumor virotherapy.

References

Andtbacka RH, Kaufman HL, Collichio F et al (2015) Talimogene laherparepvec improves durable response rate in patients with advanced melanoma. J Clin Oncol 33:2780–2788

Araujo RP, McElwain LS (2004) A history of the study of solid tumor growth: the contribution of mathematical modeling. Bull Math Biol 66:1039–1091

Chaplain M, Kuznetsov V, James Z, Stepanova A (1998) Spatio-temporal dynamics of the immune system response to cancer. In: Horn MA, Simonett G, Webb GF (eds) Mathematical models in medical and health sciences. Vanderbilt University Press, Nashville

Chiocca EA, Rabkin SD (2014) Oncolytic viruses and their application to cancer immunotherapy. Cancer Immunol Res 2:295–300

Friedman A (2007) Mathematical analysis and challenges arising from models of tumor growth. Math Models Methods Appl Sci 17:1751–1772

Friedman A, Tian JP, Fulci G, Chiocca EA, Wang J (2005) Glioma virotherapy: effects of innate immune suppression and increased viral replication capacity. Cancer Res 66:2314–2319

Fulci G, Breymann L, Gianni D et al (2006) Cyclophosphamide enhances glioma virotherapy by inhibiting innate immune responses. Proc Natl Acad Sci USA 103:12873–12878

Golub GH, Van Loan CF (2012) Matrix computations. Johns Hopkins University Press, Baltimore

Kambara H, Okano H, Chiocca EA, Saeki Y (2005) An oncolytic HSV-1 mutant expressing ICP34.5 under control of a nestin promoter increases survival of animals even when symptomatic from a brain tumor. Cancer Res 65:2832–2839

Karev GP, Novozhilov AS, Koonin EV (2006) Mathematical modeling of tumor therapy with oncolytic viruses: effects of parametric heterogeneity on cell dynamics. Biol Direct 1:30

Kasuya H, Takeda S, Nomoto S, Nakao A (2005) The potential of oncolytic virus therapy for pancreatic cancer. Cancer Gene Ther 12:725–736

Kirn DH, McCormick F (1996) Replicating viruses as selective cancer therapeutics. Mol Med Today 2:519–527

Kirn D, Hermiston T, McCormick F (1998) ONYX-015: clinical data are encouraging. Nat Med 4:1341–1342

Lawler SE, Chiocca EA (2015) Oncolytic virus-mediated immunotherapy: a combinatorial approach for cancer treatment. J Clin Oncol 33:2812–2814

Lowengrub JS, Frieboes HB, Jin F, Chuang Y-L, Li X, Macklin P, Wise SM, Cristini V (2010) Nonlinear modeling of cancer: bridging the gap bewteen cells and tumors. Nonlinearity 23:R1–R91

Marchini A, Scott EM, Rommelaere J (2016) Overcoming barriers in oncolytic virotherapy with HDAC inhibitors and immune checkpoint blockade. Viruses 8(1):9

Melcher A, Parato K, Rooney CM, Bell JC (2011) Thunder and lightning: immunotherapy and oncolytic viruses collide. Mol Ther 19:1008–1016

Novozhilov AS, Berezovskaya FS, Koonin EV, Karev GP (2006) Mathematical modeling of tumor therapy with oncolytic viruses: regimes with complete tumor elimination within the framework of deterministic models. Biol Direct 1:6

Parish CR, O'Neill ER (1997) Dependence of the adaptive immune response on innate immunity: some questions answered but new paradoxes emerge. Immunol Cell Biol 75:523–527

Parato KA, Senger D, Forsyth PA, Bell JC (2005) Recent progress in the battle between oncolytic viruses and tumours. Nat Rev Cancer 5:965–976

Pecora AL, Rizvi N, Cohen GI et al (2002) Phase I trial of intraveneous administration of PV701, an oncolytic virus, in patients with advanced solid cancers. J Clin Oncol 20:2251–2266

Press WH, Flannery BP, Teukolsky SA, Vetterling WT (1996) Numerical recipes in Fortran 90. Cambridge University Press, New York

Shah AC, Benos D, Gillespie GY, Markert JM (2003) Oncolytic viruses: clinical applications as vectors for the treatment of malignant gliomas. J Neurooncol 65:203–226

Tian JP (2011) The replicability of oncolytic virus: defining conditions on tumor virotherapy. Mathe Biosci Eng 8:841–860

Wang J, Tian JP (2008) Numerical study for a model of tumor virotherapy. Appl Math Comput 196:448–457

Wodarz D (2001) Viruses as antitumor weapons: defining conditions for tumor remission. Cancer Res 61:3501–3507

Wodarz D, Komarova N (2005) Computational biology of cancer: lecture notes and mathematical modeling. World Scientific Publishing Company, Singapore

Woller N, Gürlevik E, Ureche C-I, Schumacher A, Kühnel F (2014) Oncolytic viruses as anticancer vaccines. Front Oncol 4:188

Wu JT, Byrne HM, Kirn DH, Wein LM (2001) Modeling and analysis of a virus that replicates selectively in tumor cells. Bull Math Biol 63:731–768

World Cancer Report (2014a) Chapter 1.1. World Health Organization, 2014

World Cancer Report (2014b) Chapter 6.7. World Health Organization, 2014